Available online at www.sciencedirect.com
SCIENCE DIRECT®
Journal of Molecular Catalysis A: Chemical 223 (2004) 167–176
JOURNAL OF MOLECULAR CATALYSIS A: CHEMICAL
www.elsevier.com/locate/molcata

Mesolamellar vanadium phosphate phases obtained by intercalation of a long chain alkylamine into different catalytically important VPO host lattices

Soumen Dasgupta, Monika Agarwal, Arunabha Datta*

Analytical Sciences Division, Indian Institute of Petroleum, P.O. IIP Mohkhampur, Dehra Dun 248005, India

Received 8 March 2003; received in revised form 10 September 2003; accepted 20 September 2003
Available online 11 September 2004

Abstract

The intercalation of octadecyl amine (ODA) into the catalytically important $VOHPO_4{\cdot}4H_2O$, $VOHPO_4{\cdot}0.5H_2O$, $VOPO_4{\cdot}2H_2O$ and $VOHPO_3{\cdot}1.5H_2O$ phases has been found to give rise to mesolamellar phases with basal spacings of 32.8, 36.3, 30.0 and 36.2 Å, respectively. It is shown from FTIR and CP-MAS NMR studies that considerable disorder in the alkyl tail of the intercalated ODA is introduced due to the internal methylene groups assuming *gauche* conformations. Consequently, the observation that the interlayer spacing of the ODA intercalates is lower than that expected from a fully stretched ODA molecule can be ascribed to the fact that the *gauche* conformations of the internal methylene groups cause a shortening of the effective length of the molecule. This contradicts the postulation of tilted configurations of fully stretched all *trans* alkyl amine molecules made in earlier studies of alkyl amine intercalation in VPO phases. It is also observed that the extent of conformational disorder in the intercalated ODA molecules is dependent on the structure of the host VPO lattice with the highest conformational disorder in the ODA intercalate of $VOHPO_4{\cdot}4H_2O$ followed by the intercalates of $VOHPO_4{\cdot}0.5H_2O$, $VOPO_4{\cdot}2H_2O$ and $VOHPO_3{\cdot}1.5H_2O$.

Keywords: Mesolamellar; Vanadium phosphates; Intercalation; Alkylamine; Orientation

1. Introduction

Vanadium phosphorous oxides (VPO's) are a class of layered solids that exist in different structural and topological modifications due to variations in the mode of bonding, spatial orientations and nature of cross-linking between the octahedral vanadyl and the tetrahedral phosphate or phosphite structural units [1]. Some of the VPO phases have tremendous technological importance as catalysts for the selective oxidation of butane to maleic anhydride as well as for their potential industrial application in the selective conversion of propane to acrylic acid, pentane to phthalic anhydride and ammoxidation of various alkyl aromatics to the corresponding aromatic nitriles [2]. Amongst them, the vanadium (IV) phases, vanadyl hydrogen phosphate hemihydrate $VOHPO_4{\cdot}0.5H_2O$, vanadyl hydrogen phosphate tetrahydrate $VOHPO_4{\cdot}4H_2O$, vanadyl phosphite $VOHPO_3{\cdot}1.5H_2O$ and the vanadium (V) phase, vanadyl phosphate dihydrate $VOPO_4{\cdot}2H_2O$ are industrially very important as precursors to the vanadyl pyrophosphate $(VO)_2P_2O_7$ phase which has been established to be the catalytically active phase in the selective oxidation of butane to maleic anhydride.

The catalytic activity of the $(VO)_2P_2O_7$ phase is known to be very sensitive to its structural and morphological characteristics which in turn can be controlled through the precursor phase [3]. The four precursors to the pyrophosphate phase are structurally quite different. Thus the structure of vanadyl (V) orthophosphate, $VOPO_4{\cdot}2H_2O$ is made up of corner shared VO_6 octahedra and PO_4 tetrahedra forming a two-dimensional layer lattice [4], whereas face shared vanadyl dimers are interconnected by corner sharing with

* Corresponding author. Tel.: +91 135 2660 263; fax: +91 135 2660 202.
E-mail address: adatta@iip.res.in (A. Datta).

1381-1169/$ – see front matter © 2004 Published by Elsevier B.V.
doi:10.1016/j.molcata.2003.09.043

Table 1
Compositional analysis of the VPO-ODA intercalates

Sample code	Parent host	ODA content (wt.%)[a]	P (wt.%)[b]	V (wt.%)[b]	O (wt.%)[c]	H_2O (wt.%)[d]	Composition
ODA-VP0.5	$VOHPO_4{\cdot}0.5H_2O$	51.59	9.00	14.82	23.54	1.05	$(ODA)_{0.66}VOHPO_4{\cdot}0.2H_2O$
ODA-VP1.5	$VOHPO_3{\cdot}1.5H_2O$	63.67	7.39	12.16	15.49	1.29	$(ODA)_{0.77}VOHPO_3{\cdot}0.3H_2O$
ODA-VP2	$VOPO_4{\cdot}2H_2O$	53.95	8.40	13.82	21.68	2.15	$(ODA)_{0.74}VOPO_4{\cdot}0.44H_2O$
ODA-VP4	$VOHPO_4{\cdot}4H_2O$	53.93	7.97	13.11	20.83	4.16	$(ODA)_{0.78}VOHPO_4{\cdot}0.9H_2O$

[a] Amine content was determined from TGA considering mass loss above 423 K due to the loss of alkyl amine surfactant.
[b] P and V content was determined by ICP analysis.
[c] O% = 100 − (%P + %V + $\%H_2O$ + %amine).
[d] H_2O content was determined from TGA considering mass loss in the region 303–423 K due to loss of H_2O.

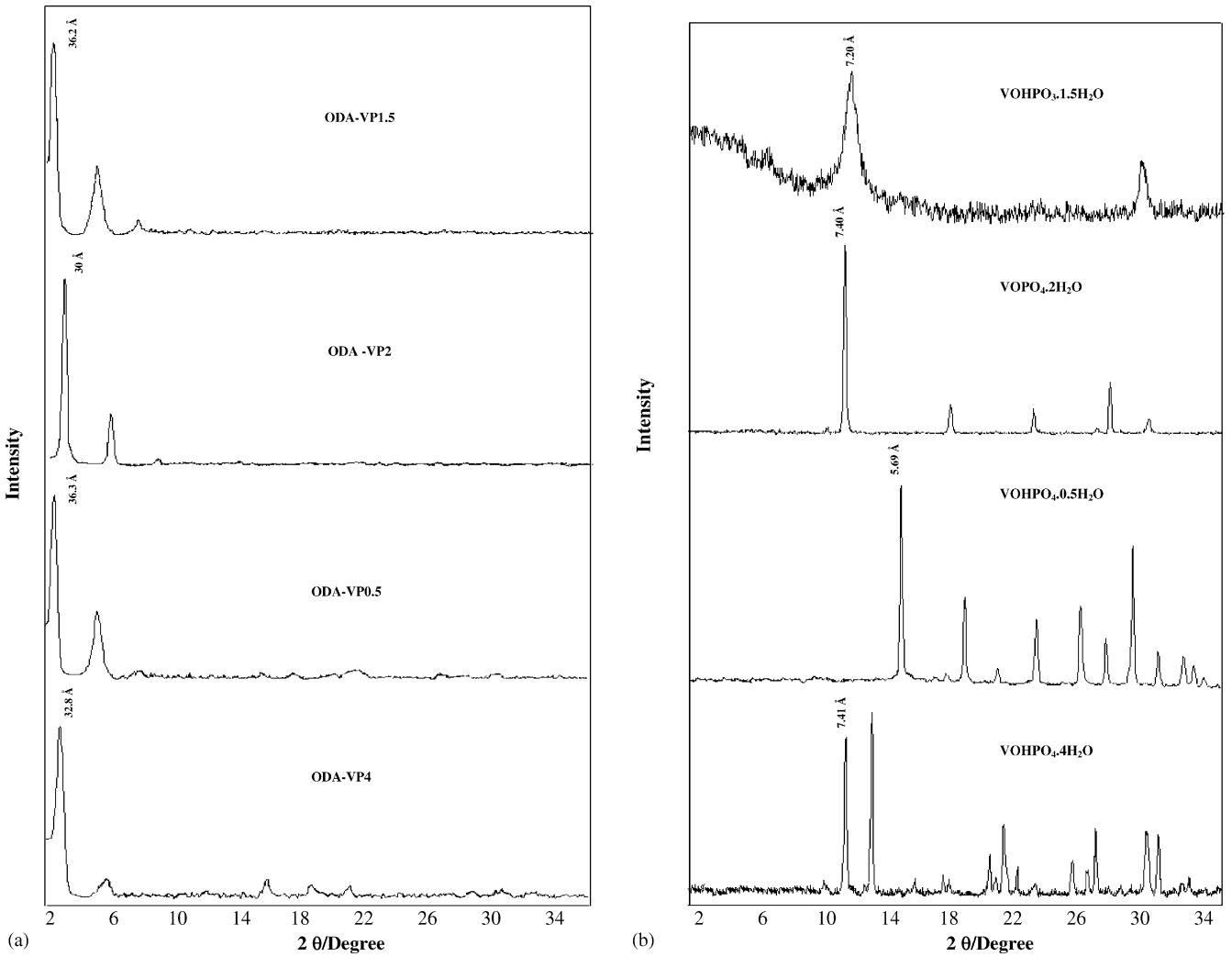

Fig. 1. (a) XRD patterns of the intercalation products of octadecyl amine (ODA) with $VOHPO_4{\cdot}4H_2O$ (ODA-VP4), $VOHPO_4{\cdot}0.5H_2O$ (ODA-VP0.5), $VOPO_4{\cdot}2H_2O$ (ODA-VP2) and $VOHPO_3{\cdot}1.5H_2O$ (ODA-VP1.5). (b) XRD patterns of parent VPO host phases.

hydrogen phosphate (HPO_4) groups in vanadyl (IV) hydrogen phosphate hemihydrate [5,6], $VOHPO_4{\cdot}0.5H_2O$ and by hydrogen phosphite (HPO_3) groups in the vanadyl hydrogen phosphite $VOHPO_3{\cdot}1.5H_2O$ phase [7]. The vanadyl hydrogen phosphate tetrahydrate ($VOHPO_4{\cdot}4H_2O$) on the other hand has a completely different structure formed by a double chain arrangement of corner shared VO_6 and HPO_4 polyhedral units [6]. The layers of $VOPO_4{\cdot}2H_2O$ and the double chains of $VOHPO_4{\cdot}4H_2O$ are loosely stacked together by weak hydrogen bonding interaction involving vanadium bound water and interlayer residing free zeolithic water molecules [4,6]. In contrast there is a tight interlayer binding [5,6] in $VOHPO_4{\cdot}0.5H_2O$ due to the existence of a hydrogen-bonding network in the interlayer region. The layers of $VOHPO_3{\cdot}1.5H_2O$, however are less tightly held in comparison to the hemihydrate phase.

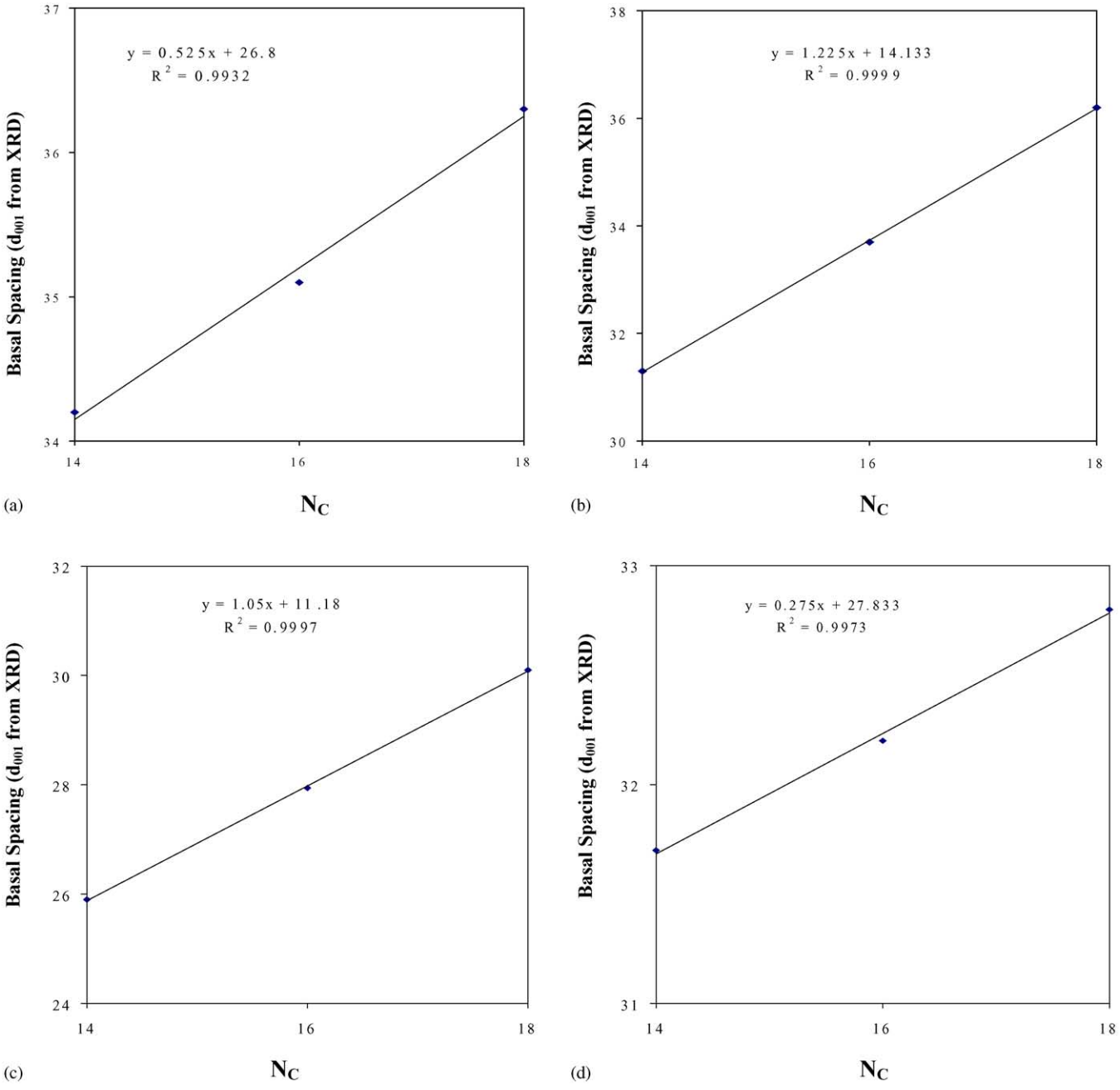

Fig. 2. Plots showing variation of basal spacing (d_{001} from XRD) with the number of carbon atoms (N_C) for alkyl amines of different chain lengths viz. *n*-C_{14}, *n*-C_{16} and *n*-C_{18} intercalated into $VOHPO_4{\cdot}0.5H_2O$ (a), $VOHPO_3{\cdot}1.5H_2O$ (b), $VOPO_4{\cdot}2H_2O$ (c) and $VOHPO_4{\cdot}4H_2O$ (d).

The intercalation compounds of layered vanadium orthophosphates are of tremendous interest not only as fundamental examples of V–P–O nanocomposites but also as intermediates for constructing novel V–P–O nanostructures of catalytic importance [7]. Owing to the weak interlayer binding in $VOPO_4{\cdot}2H_2O$ and $VOHPO_4{\cdot}4H_2O$, these solids can act as host to different guest molecules. In this context $VOPO_4{\cdot}2H_2O$ has been shown to be very amenable for intercalation of alcohols [8], aliphatic and aromatic amines [9], pyridine and its derivatives [9i,10], organometallic compounds [11], glycols [12] and amides [13]. $VOPO_4{\cdot}2H_2O$ is also known to undergo redox intercalation of metal ions [14]. In contrast the intercalation chemistry of $VOHPO_4{\cdot}4H_2O$ has hardly been studied and apart from the incorporation of some small chain alkyl amines [7,9c,15], attempts to intercalate other molecules into the $VOHPO_4{\cdot}0.5H_2O$ and $VOHPO_3{\cdot}1.5H_2O$ phases have not been very successful due to their less open interlayer structure, although some interesting phase transformations during metal ion incorporation into $VOHPO_4{\cdot}0.5H_2O$ have been reported [16].

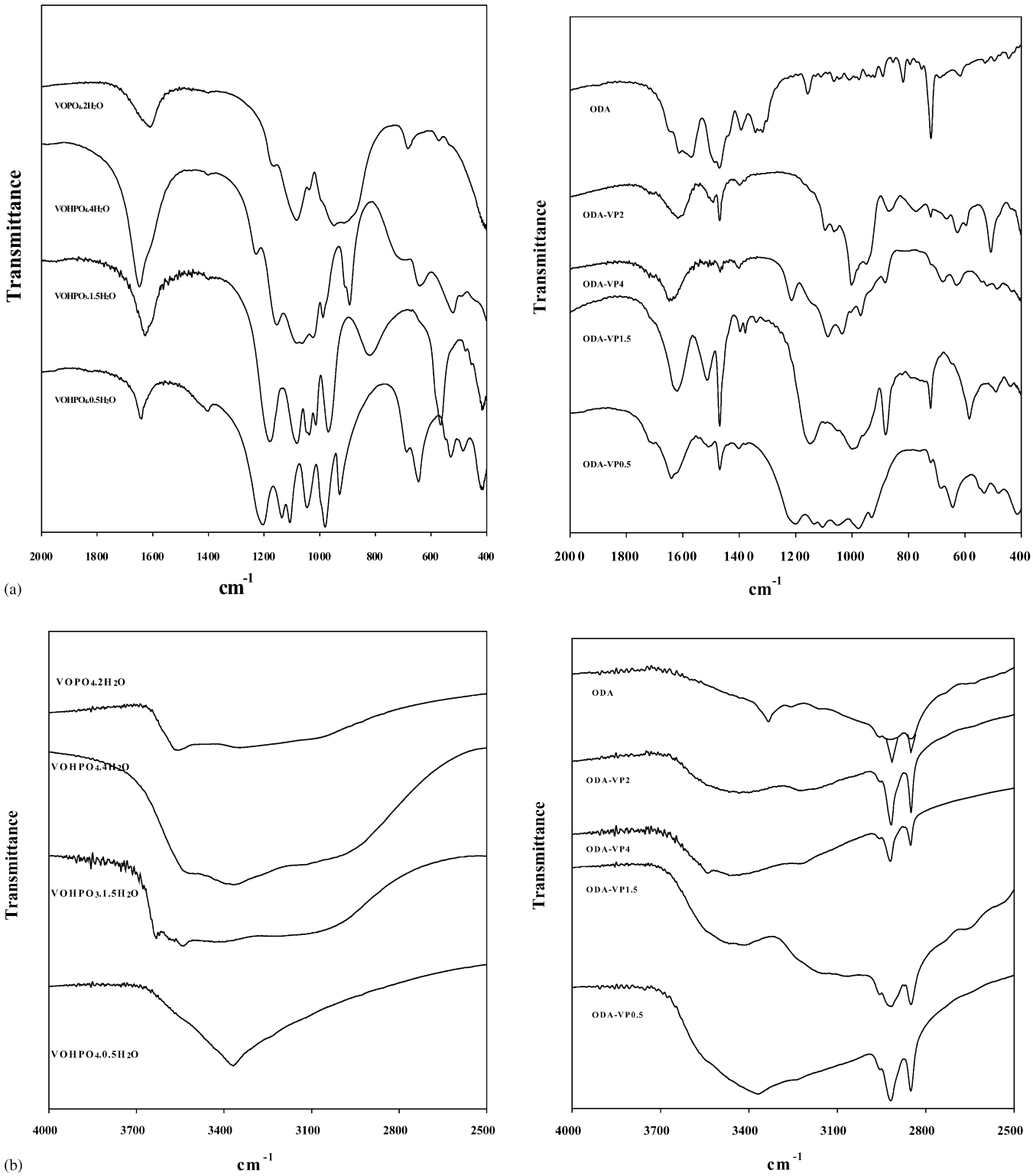

Fig. 3. (a) FTIR patterns of different VPO hosts and their corresponding ODA intercalation products in the range 400–2000 cm^{-1}. (b) FTIR pattern of different VPO hosts and their corresponding ODA intercalation products in the range 2500–4000 cm^{-1}.

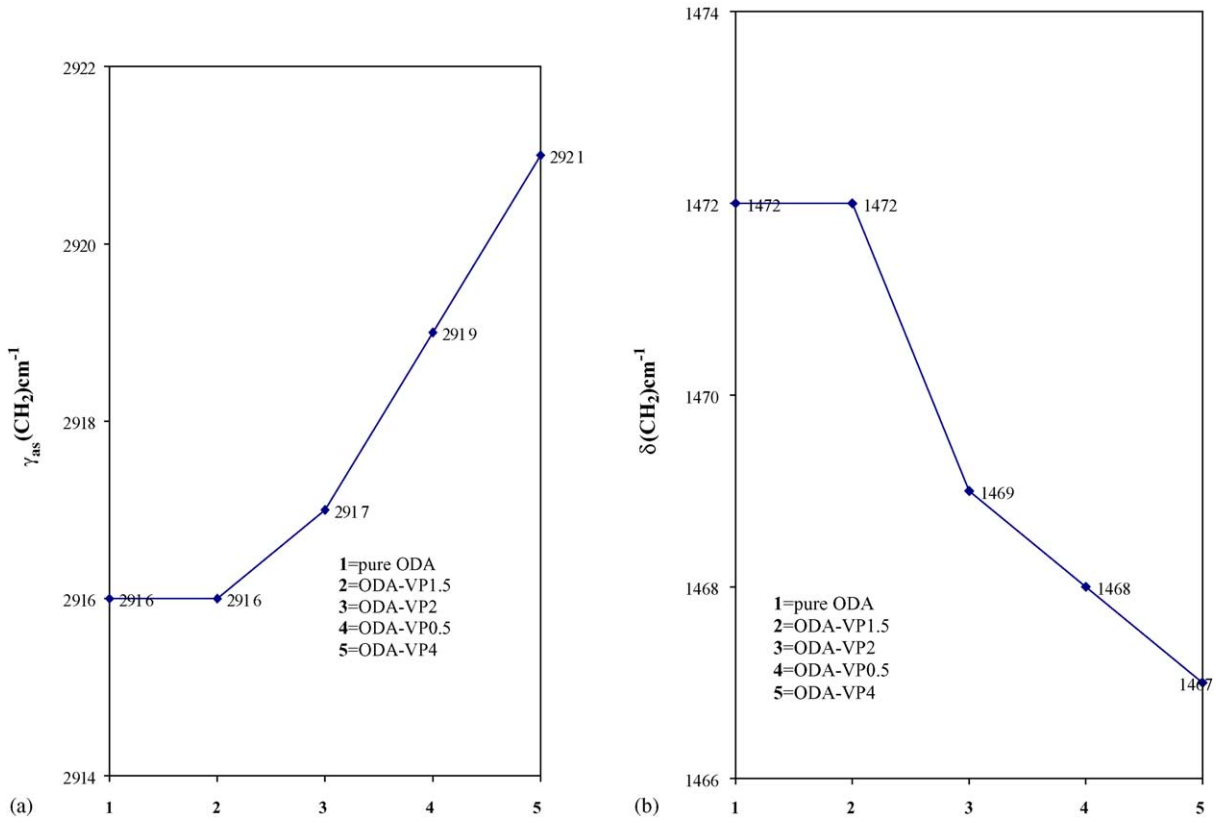

Fig. 4. (a) Plot showing variation of $\gamma_{as}CH_2$ frequency in pure ODA and in ODA intercalated into different VPO hosts. (b) Plot showing variation of δCH_2 frequency in pure ODA and in ODA intercalated into different VPO hosts.

The intercalation of long chain alkyl amine molecules into layered VPO solids leads to the formation of lamellar VPO phases of mesoscopic dimensions [17]. These novel nanofabricated VPO materials are of interest because of their unique structure and potential use in catalysis. So far though no systematic study has been done to understand the orientation of the incorporated amine molecules in VPO-amine nanocomposites. This knowledge would be essential in order to tailor the structural properties of these solids as we have shown recently that subtle changes in the conformational orientation of the incorporated alkyl amine surfactants can lead to profound differences in the layer packing and interlayer distance in mesostructured VPO materials [18]. In the present work therefore we have studied the intercalation of a long chain amine such as octadecyl amine (ODA) into the four different VPO phases namely $VOHPO_3{\cdot}1.5H_2O$, $VOHPO_4{\cdot}0.5H_2O$, $VOHPO_4{\cdot}4H_2O$ and $VOPO_4{\cdot}2H_2O$ with the aim of investigating the effect of the structure of the host VPO lattice on the orientation and conformation of the intercalated amine molecules.

2. Experimental

$VOPO_4{\cdot}2H_2O$, $VOHPO_4{\cdot}0.5H_2O$, $VOHPO_4{\cdot}4H_2O$ and $VOHPO_3{\cdot}1.5H_2O$ were synthesized by following literature methods [7,19] and were characterized by XRD, FTIR, TGA and elemental analysis. Intercalation of alkyl amines such as *n*-octadecyl amine (ODA), *n*-hexadecyl amine and *n*-tetradecyl amine into $VOPO_4{\cdot}2H_2O$, $VOHPO_3{\cdot}1.5H_2O$, $VOHPO_4{\cdot}4H_2O$ and $VOHPO_4{\cdot}0.5H_2O$ were done under identical conditions by stirring the above solids in the homogeneous dispersion of any of the alkyl amines in water or in a mixture of dimethyl formamide (DMF) and water. DMF-water mixture was used as the reaction medium in the case of $VOHPO_4{\cdot}0.5H_2O$ as complete intercalation of the alkyl amines in $VOHPO_4{\cdot}0.5H_2O$ was achieved only in this medium after a reaction time of 24 h. In a representative procedure of intercalation, 5 mmol of $VOHPO_4{\cdot}0.5H_2O$ was dispersed into the homogeneous dispersion of 1.25 mmol of ODA in a 40 ml mixture of distilled water and DMF (1:1 (v/v)). The slurry was stirred at 353 K for 24 h and the product isolated by filtration. The solid was thoroughly washed with acetone to remove any unreacted alkyl amine and dried in an air oven at 393 K for 6 h. Intercalation of the alkyl amines into other solids was done by stirring the respective solids in 40 ml aqueous dispersion of alkyl amine, maintaining other conditions exactly the same. The products obtained by the intercalation of ODA into $VOPO_4{\cdot}2H_2O$, $VOHPO_3{\cdot}1.5H_2O$, $VOHPO_4{\cdot}4H_2O$ and $VOHPO_4{\cdot}0.5H_2O$ were coded as ODA-VP2, ODA-VP1.5, ODA-VP4 and ODA-VP0.5, respectively.

3. Chemical and physical measurements

The X-ray powder diffractograms were recorded at room temperature on a GE XRD 9530 diffractometer using Cu Kα radiation (λ = 1.5406 Å) and were scanned in the 2θ region 2° to 50° at the rate of 2°/min. FTIR spectra were recorded on a Perkin-Elmer 1760X FTIR spectrometer with the sample powder diluted in KBr (1%). Typically 100 scans with a resolution of 2 cm^{-1} were collected for each sample. All the solid-state ^{13}C CP-MAS NMR experiments were performed at room temperature on a Bruker Avance 500 NMR spectrometer operating at resonance frequencies of 125.75 MHz for ^{13}C and 500.13 MHz for ^{1}H, respectively. Finely powdered samples were loaded in 4 mm zirconia rotors and were put in the CP-MAS probe. CP-MAS experiments were performed with a standard CP sequence with TPPM decoupling [20] scheme during the acquisition period for most efficient hetero nuclear decoupling. A π/2 pulse of 5 μs was applied to the protons to create the transverse ^{1}H magnetization at the spinning frequency of 8 kHz. This 8 kHz sample spinning was sufficient for removing the anisotropic part of various spin interactions, specifically for CSA. Contact pulses of 250 μs were applied in both ^{1}H and ^{13}C channels with Hartmann–Hahn matching condition at 50 kHz rf field for polarization transfer in rotating frame under spin-lock condition. In the pulse sequence, ^{1}H spin temperature alternation was done with alternatively shifting rf phase by 180° for ^{1}H rf pulse and receiver phase cycling for CYCLOPS was implemented for all spectral recordings. The number of scans of FID were varied from 1000 to 3200 depending on samples in order to get optimum signal to noise ratios. All spectra were processed with glycine as the external reference. In order to obtain more detailed information about internal methylene peaks, Bruker's interactive solid-state deconvolution method was applied for the broad spectral region 26–40 ppm. For the individual peaks with their respective isotropic chemical shift values (δ_{iso}), appropriate Gaussian/Lorentzian convolution factors were applied for each spectra separately. Individual peak positions, line widths and peak intensities were used as variable parameters in iterations till the best fit for each spectra were obtained. Thermogravimetric analysis was carried out using a Mettler TG-50 model and the DSC patterns were recorded on a Mettler DSC-20 model using a heating rate of 10 K/min and an airflow of 150 ml/min. The composition analysis of the VPO-ODA intercalates is presented in Table 1.

4. Results and discussions

4.1. XRD

XRD patterns of the ODA intercalation products (Fig. 1a) of $VOHPO_4{\cdot}4H_2O$ (ODA-VP4), $VOHPO_4{\cdot}0.5H_2O$ (ODA-VP0.5), $VOPO_4{\cdot}2H_2O$ (ODA-VP2) and $VOHPO_3{\cdot}1.5H_2O$ (ODA-VP1.5) show complete transformation of these solids to mesolamellar phases as no diffraction lines due to the parent VPO solids are observed in the products (Fig. 1b). All the XRD patterns are characteristic of single mesolamellar phases with basal spacings (d_{001} from XRD) of 32.8, 36.3, 30.0 and 36.2 Å, respectively. All these phases also display the corresponding (002) and (003) reflections in their XRD patterns, except in the case of ODA-VP4 where the (003) reflection is not observed but additional lines, not due to the parent compound, are present.

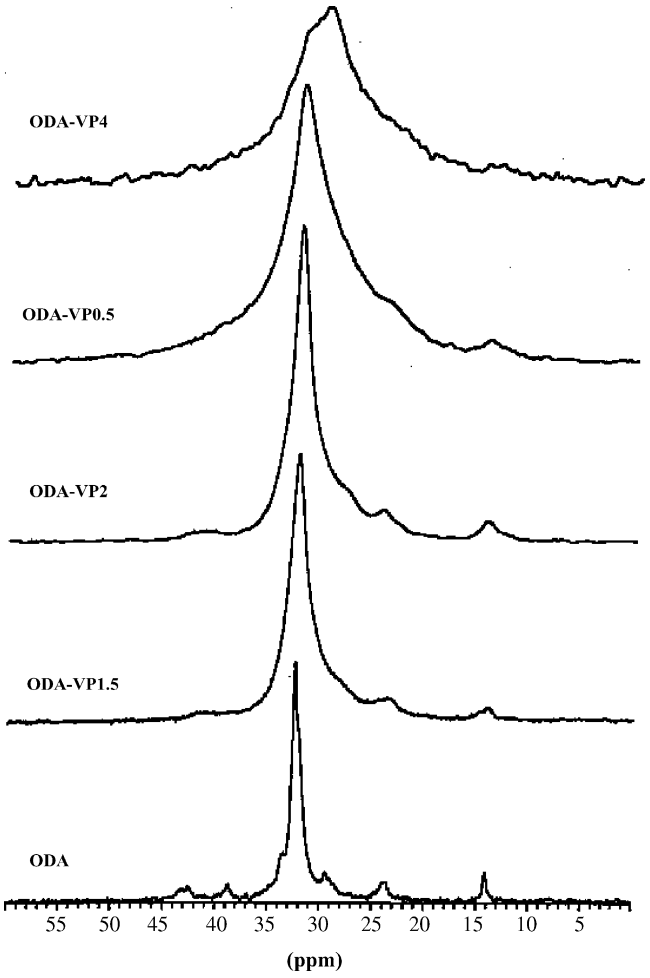

Fig. 5. ^{13}C CP-MAS NMR spectra of pure solid ODA and the intercalation products of ODA with different VPO hosts.

In order to ascertain the arrangement of ODA molecules in the intercalates, two additional alkyl amines with chain lengths of n-C_{14} and n-C_{16} were also intercalated into the four different VPO phases. The basal spacing (d_{001}) determined from the XRD patterns of these phases along with the ODA intercalated phase were then plotted against the carbon numbers of the alkyl amines for each individual host. Good least square fits (Fig. 2) with slope values of 0.275, 0.525, 1.05 and 1.225 Å/CH_2 were obtained for alkyl amine intercalation products of $VOHPO_4{\cdot}4H_2O$, $VOHPO_4{\cdot}0.5H_2O$ $VOPO_4{\cdot}2H_2O$ and $VOHPO_3{\cdot}1.5H_2O$, respectively. For a monolayer arrangement of alkyl chains in an

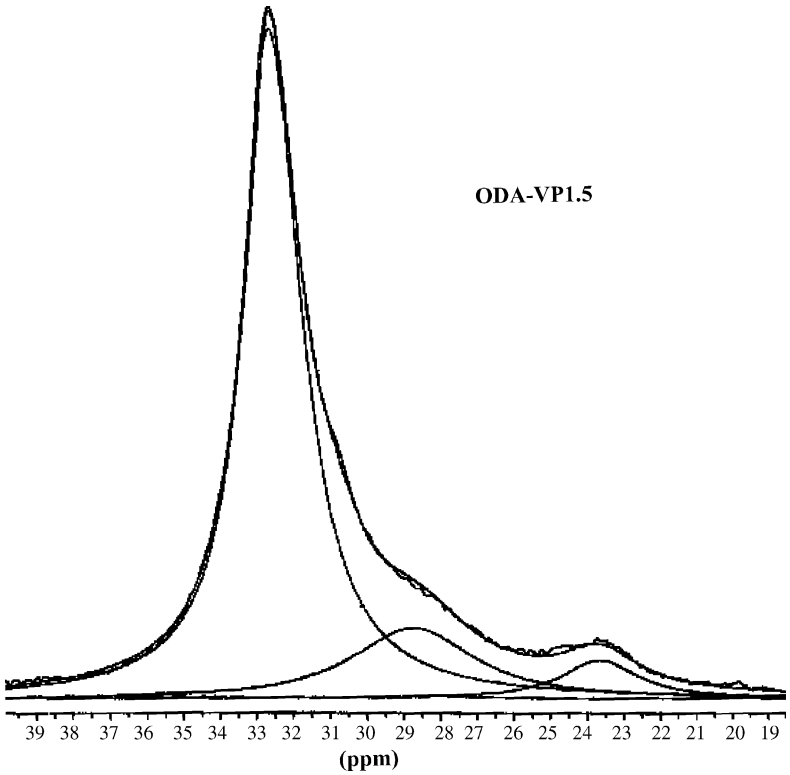

Fig. 6. Deconvoluted ^{13}C CP-MAS NMR spectra (40–18 ppm region) of the ODA intercalate of $VOHPO_3{\cdot}1.5H_2O$ (ODA-VP1.5).

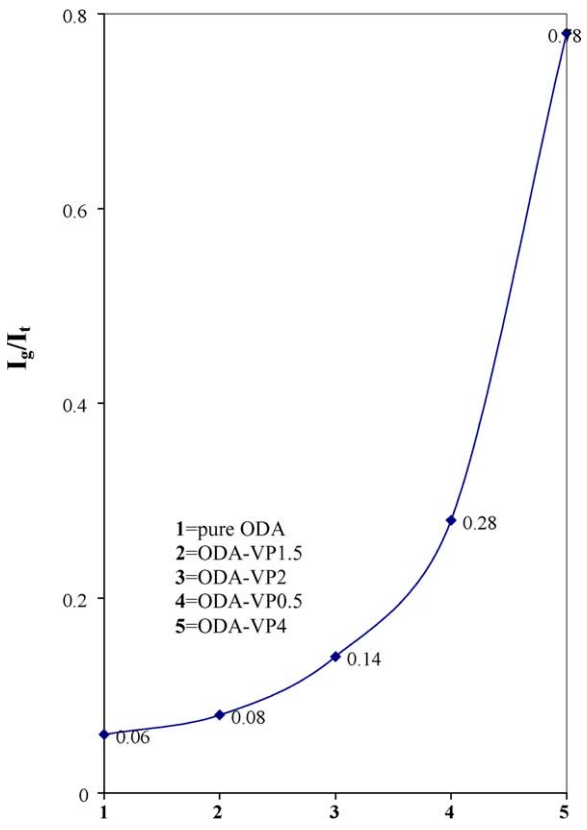

Fig. 7. Plot showing variation of the NMR intensity ratio due to the *gauche* (I_g) and *trans* (I_t) domain i.e. I_g/I_t in pure ODA and the intercalation products of ODA with different VPO hosts.

all *trans* conformation, oriented perpendicularly with respect to the *ab* basal plane of the inorganic layer, the theoretical increase of basal spacing [21] for addition of each methylene group should be 1.27 Å. The experimentally obtained values for the increase in basal spacing for each methylene group in the alkyl amine intercalates are thus quite different for the various host lattices. Also, the values for the thickness of the inorganic layer obtained by the extrapolation of the plots in Fig. 2 for the intercalates of $VOHPO_4{\cdot}4H_2O$, $VOHPO_4{\cdot}0.5H_2O$, $VOPO_4{\cdot}2H_2O$, and $VOHPO_3{\cdot}1.5H_2O$ are 27.8, 26.8, 11.2 and 14.1 Å, respectively indicating large variations in the inorganic layer thickness amongst the mesolamellar VPO phases from the four different VPO hosts.

4.2. FTIR

FTIR spectra of ODA-VP2 in the P–O, V–O stretching region (800–1300 cm^{-1}) show changes in the V–P–O connectivity of the parent $VOPO_4{\cdot}2H_2O$ phase following ODA intercalation. In contrast the V–P–O connectivity of the respective parent hosts are largely retained in ODA-VP0.5, ODA-VP1.5 and ODA-VP4 as is evident from their band structure in the P–O, V–O stretching region (Fig. 3a). An insight into the conformation of the ODA molecules in the intercalates can be obtained from the analysis of the band positions in the methylene stretching γ_{as} (CH_2) and bending δ (CH_2) modes of the interior methylene groups in the alkyl tail of the incorporated ODA molecules (Fig. 3b). In pure ODA, bands at 2916 and 1472 cm^{-1}, correspond to the

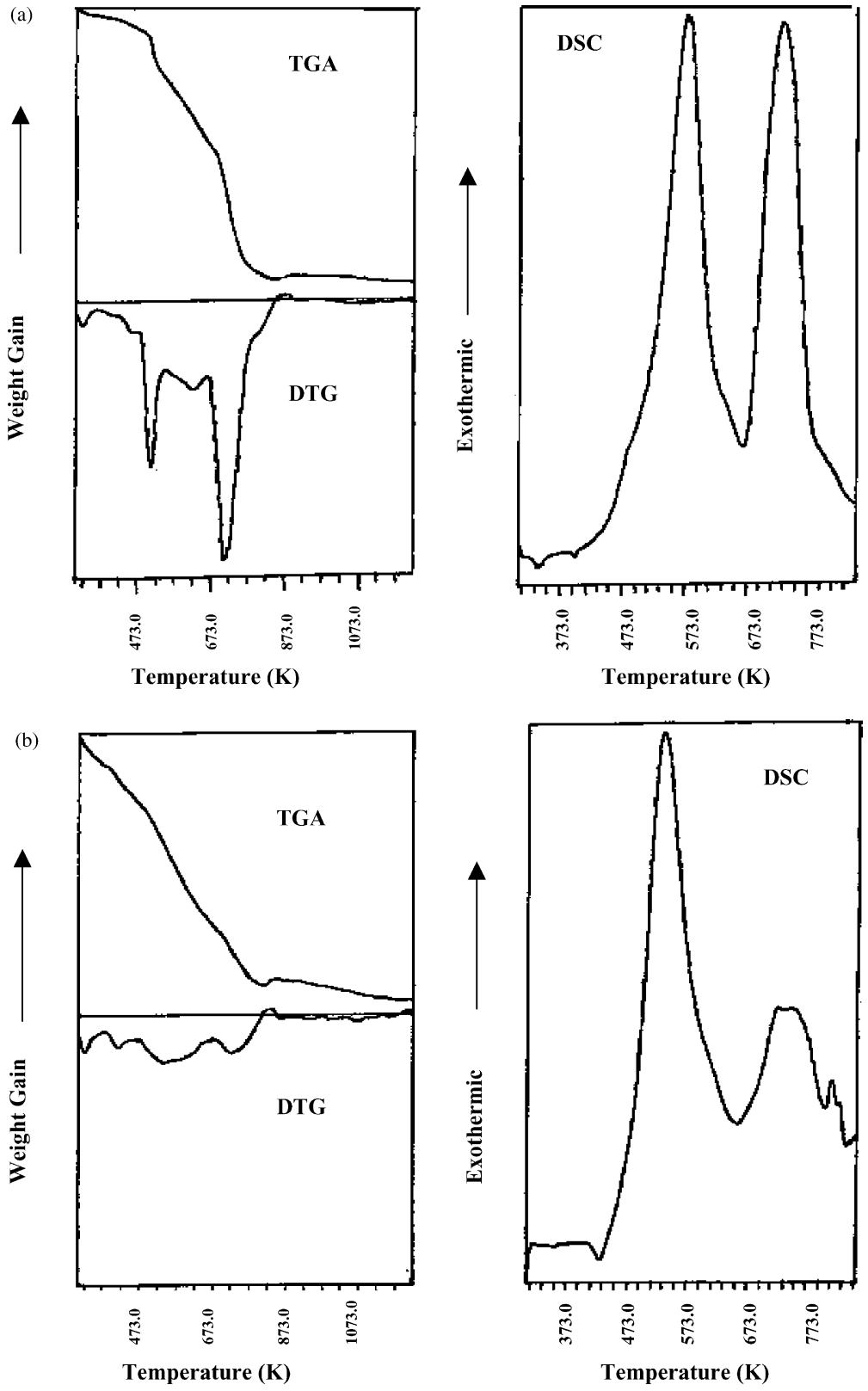

Fig. 8. TGA/DTG and DSC patterns of the intercalation products of ODA with $VOHPO_3 \cdot 1.5H_2O$ with (a) $VOHPO_3 \cdot 1.5H_2O$ and (b) $VOHPO_4 \cdot 4H_2O$.

asymmetric stretching, γ_{as} (CH_2) and bending, δ (CH_2) vibrations of an all *trans* conformation of the internal methylene groups in the alkyl tail. The positions of these bands are known to be sensitive to the *gauche*/*trans* conformer ratio in the alkyl group of surfactants with an increase in the ordering of the alkyl tail with increasing *trans* conformation of the interior methylene groups leading to small bathochromic shifts in the γ_{as} (CH_2) vibration and to small hypsochromic shifts in the δ (CH_2) vibration [22]. The variation of γ_{as} (CH_2) and δ (CH_2) frequencies in pure ODA and the VPO intercalates (Fig. 4a and b) indicate that the increase in the conformational disorder in the methylene chains of the ODA molecules follows the sequence ODA-VP4 > ODA-VP0.5 > ODA-VP2 > ODA-VP1.5 ∼ ODA (pure).

4.3. ^{13}C CP-MAS NMR

The solid state ^{13}C CPMAS NMR spectrum of pure octadecyl amine (ODA) shows isotropic chemical shifts of 43 and 39 ppm assignable to the carbon (C_1) adjacent to the amine head group and the carbon (C_2) next to it, respectively. On intercalation of ODA into $VOPO_4{\cdot}2H_2O$, $VOHPO_3{\cdot}1.5H_2O$, $VOHPO_4{\cdot}4H_2O$ and $VOHPO_4{\cdot}0.5H_2O$ the signals due to C_1 and C_2 are no longer visible as distinct peaks (Fig. 5). This indicates strong interaction of the amine head group of the octadecyl amine molecule with the VPO matrix in the intercalates. This is because such an interaction would make the alkyl amine molecules in their intercalated state more rigid. The resulting increase of residual dipolar and chemical shift anisotropic interactions would be felt more by the C_1 and C_2 carbons because of their highest rigidity by virtue of their close proximity to the inorganic lattice and hence their ^{13}C NMR signal would be very broad and weak in intensity.

The conformational heterogeneity of the ODA intercalated VPO phases was also probed by ^{13}C CP-MAS NMR spectroscopy. For long chain alkyl group containing surfactants a ^{13}C NMR signal in the chemical shift range 32–34 ppm indicates the presence of highly ordered all *trans* domain while a peak in the range 28–30 ppm corresponds to the disordered *gauche* domain in the interior methylene groups of the alkyl group [23]. It is evident that the ^{13}C CP-MAS NMR spectra of the ODA intercalates have structured band patterns due to superimposed peaks in the range 20–40 ppm. By deconvolution of the ^{13}C NMR spectra in this region, the ratio of the area intensity due to the *gauche* (I_g) and *trans* (I_t) signal was estimated for pure ODA and for each ODA intercalate. A typical deconvoluted spectrum is shown in Fig. 6. Variation of the I_g/I_t ratio from pure ODA molecules to the various ODA intercalates is shown in Fig. 7. A gradual increase in the conformational disorder in the intercalated ODA molecules according to the sequence ODA-VP4 > ODA-VP0.5 > ODA-VP2 > ODA-VP1.5 ∼ ODA is evident in agreement with the FTIR data.

4.4. Thermal analysis

TG and derivative TG (DTG) patterns of the ODA intercalates showed weight loss peaks below 423 K due to the loss of water. Subsequently all the samples showed weight loss peaks in the temperature range 423–823 K which could be attributed to a complex multi step decomposition of the incorporated amines. A similar decomposition behavior of amine surfactants has been observed earlier [17]. In ODA-VP1.5, in this temperature range (Fig. 8) there are weight loss peaks at 507, 583 and 713 K. Correspondingly its DSC (Fig. 8) pattern shows a shoulder at 503 K and two exothermic peaks at 578 and 720 K The three weight loss peaks in ODA-VP1.5 with corresponding exothermic peaks in the DSC pattern, can be attributed to the stepwise loss of the intercalated amine through oxidation. Very similar TGA/DTG and DSC patterns were observed for ODA-VP2 and ODA-VP0.5 with small variations in the mass loss and exothermic peak positions. In contrast, no distinct mass loss peaks were observed in the case of ODA-VP4. Instead, very broad mass loss peaks centered at 533 and 723 K were observed (Fig. 8) which is in keeping with the fact that ODA molecules are in the most disordered state in ODA-VP4 as evidenced by FTIR and NMR studies.

5. Conclusions

The intercalation of ODA into different VPO host lattices gives rise to mesolamellar phases with wide variations in the conformation of the incorporated ODA. It is shown that considerable disorder in the alkyl tail of the intercalated ODA is introduced due to the internal methylene groups assuming *gauche* conformations. Consequently the observation that the interlayer spacing of the ODA intercalates is lower than that expected from a fully stretched ODA molecule can be ascribed to the fact that the *gauche* conformations of the internal methylene groups cause a shortening of the effective length of the molecule. This contradicts the postulation of tilted configurations of fully stretched all *trans* alkyl amine molecules made in earlier studies of alkyl amine intercalation in VPO hosts [7,15,24]. Thus a perpendicular monolayer orientation with varying degrees of conformational disorder in the alkyl tail would be the most likely arrangement of the incorporated ODA molecules in the intercalates of $VOHPO_4{\cdot}4H_2O$ $VOHPO_4{\cdot}0.5H_2O$, $VOPO_4{\cdot}2H_2O$ and $VOHPO_3{\cdot}1.5H_2O$.

On the other hand it is also obvious that the structure of the host VPO phase has a marked effect on the extent of conformational disorder in the intercalated ODA molecules. The highest conformational disorder was observed in the ODA intercalate of $VOHPO_4{\cdot}4H_2O$ followed by the intercalates of $VOHPO_4{\cdot}0.5H_2O$, $VOPO_4{\cdot}2H_2O$ and $VOHPO_3{\cdot}1.5H_2O$. The highest conformational disorder in the $VOHPO_4{\cdot}4H_2O$ intercalate can probably be attributed to the fact that $VOHPO_4{\cdot}4H_2O$ has an open one-dimensional (1D) double chain structure with ordering of the P–O–V

connectivity only along one crystallographic direction and such a 1D open structure is expected to give maximum conformational freedom and least efficient packing of the incorporated ODA molecules in the interchain region in comparison to the ODA molecules in the interlayer region of the two-dimensional (2D) hosts like $VOHPO_4{\cdot}0.5H_2O$, $VOPO_4{\cdot}2H_2O$ and $VOHPO_3{\cdot}1.5H_2O$. Among the 2D hosts, ODA is in the most disordered state in the intercalation product of $VOHPO_4{\cdot}0.5H_2O$. This is probably a consequence of the tight hydrogen bonding network structure in the interlayer region of $VOHPO_4{\cdot}0.5H_2O$, which would hinder the efficient packing of the methylene chains of the incorporated ODA molecules. The absence of such strong network of hydrogen bonds in the interlayer region of $VOPO_4{\cdot}2H_2O$ and $VOHPO_3{\cdot}1.5H_2O$ facilitates comparatively better ordering of the ODA molecules in the intercalates of these solids.

Acknowledgement

One of the authors (S.D.) is grateful to the C.S.I.R., India for the award of a Senior Research Fellowship.

References

[1] E. Bordes, Catal. Today 1 (5) (1987) 499.
[2] (a) A. Martin, B. Lucke, Catal. Today 32 (1996) 279;
(b) Z. Sobalic, S. Gonzalez Carrazon, P. Ruiz, B. Delmon, J. Catal. 185 (1999) 272.
[3] (a) G. Centi, F. Trifiro, J.R. Ebner, V.M. Franchetti, Chem. Rev. 88 (1988) 55;
(b) G. Centi (Ed.), Catal. Today, 16, 1993, and references therein;
(c) C.J. Kiely, A. Burrows, S. Sajip, G.J. Hutchings, M.T. Sananes, A. Tuel, J.C. Volta, J. Catal. 162 (1996) 31.
[4] H.R. Tietze, Aust. J. Chem. 34 (1981) 2035.
[5] C.C. Torardi, J.C. Calabrese, Inorg. Chem. 23 (1984) 1308.
[6] M.E. Leonowicz, J.W. Johnson, J.F. Brody, H.F. Shannon Jr., J.M. Newsam, J. Solid. State. Chem. 55 (1985) 370.
[7] V.V. Guliants, J.B. Benziger, S. Sundaresan, Chem. Mater. 7 (1995) 1485.
[8] L. Beneš, K. Melanová, V. Zima, J. Kalousová, J. Votinsky, Inorg. Chem. 36 (1997) 2850.
[9] (a) K. Beneke, G. Lagaly, Inorg. Chem. 22 (1983) 1503;
(b) L. Beneš, R. Hyklová, J. Kalousová, J. Votinsky, Inorg. Chim. Acta 177 (1990) 71;
(c) H. Nakajima, G. Matsubayashi, Chem. Lett. (1993) 423;
(d) A. De Stefanis, A.A.G. Tomlinson, J. Mater. Chem. 5 (1994) 105;
(e) H. Nakajima, G. Matsubayashi, J. Mater. Chem. 5 (1995) 105;
(f) A. De Stefanis, S. Foglia, A.A.G. Tomlinson, J. Mater. Chem. 5 (1995) 475;
(g) T. Yatabe, G. Matsubayashi, J. Mater. Chem. 6 (1996) 1849;
(h) T. Yatabe, M. Nakano, G. Matsubayashi, J. Mater. Chem. 8 (1998) 699;
(i) T. Nakato, Y. Furumi, N. Terao, T. Okuhara, J. Mater. Chem. 10 (2000) 737.
[10] J.W. Johnson, A.J. Jacobson, J.F. Brody, S.M. Rich, Inorg. Chem. 21 (1982) 3820.
[11] (a) S. Okuno, G. Matsubayashi, J. Chem. Soc. Dalton Trans. (1992) 2441;
(b) A. Datta, S. Bhaduri, R.Y. Kelkar, H.I. Khwaja, J. Phys. Chem. 98 (1994) 11811.
[12] K. Melánová, L. Beneš, V. Zima, R. Vahalová, Chem. Mater. 11 (1999) 2173.
[13] N. Yamamoto, T. Okuhara, T. Nakato, J. Mater. Chem. 11 (2001) 1858.
[14] (a) A.J. Jacobson, J.W. Johnson, J.F. Brody, J.C. Scanlon, J.T. Lewandouski, Inorg. Chem. 24 (1985) 1782;
(b) R. Šišková, L. Beneš, V. Zima, M. Vlacek, J. Votinsky, J. Kalousová, Polyhedron 12 (1993) 181;
(c) V. Zima, L. Beneš, R. Šišková, P. Fatena, J. Votinsky, Solid State Ionics 67 (1994) 277;
(d) V. Zima, L. Beneš, J. Votinsky, J. Kalousová, Solid State Ionics 82 (1995) 33;
(e) V. Zima, M. Kilián, M. Casciola, L. Massinelli, Chem. Mater. 11 (1999) 3258.
[15] V.V. Guliants, J.B. Benziger, S. Sundaresan, Chem. Mater. 6 (1994) 353.
[16] (a) A. Datta, A.R. Saple, R.Y. Kelkar, J. C. S. Chem. Commun. (1991) 356;
(b) A. Datta, A.R. Saple, R.Y. Kelkar, J. C. S. Chem. Commun. (1991) 1645;
(c) A. Datta, A.R. Saple, R.Y. Kelkar, J. C. S. Dalton Trans. (1994) 2145.
[17] J.E. Haskouri, S. Cabrera, M. Roca, J. Alamo, A. Beltrán-Porter, D. Beltrán-Porter, M.D. Marcos, P. Amorós, Inorg. Chem. 38 (1999) 4243.
[18] S. Dasgupta, M. Agarwal, A. Datta, J. Mater. Chem. 12 (2002) 162.
[19] (a) T. Shimoda, T. Okuhara, M. Misono, Bull. Chem. Soc. Jpn. 58 (1985) 2163;
(b) G. Ladwig, Z. Anorg. Allg. Chem. 338 (1965) 266;
(c) J.T. Wrobleski, Inorg. Chem. 27 (1988) 946.
[20] A.E. Bennett, J.H. Ok, R.G. Griffin, S. Vega, J. Chem. Phys. 96 (1992) 8624.
[21] A.I. Kitaigorodskii, Molecular Crystals and Molecules, Academic Press, New York, 1973.
[22] (a) R.A. Vaia, R.K. Teukolsky, E.P. Giannelis, Chem. Mater. 6 (1994) 1017;
(b) J. Do, A.J. Jacobson, Chem. Mater. 13 (2001) 2436.
[23] (a) W. Gao, L. Reven, Langmuir 11 (1995) 1860;
(b) L. Wang, J. Liu, G.J. Exarhos, K.Y. Flanigan, R. Bordia, J. Phys. Chem. B 104 (2000) 2810.
[24] M.S. Whittingham, A.J. Jacobson (Eds.), Intercalation Chemistry, Academic Press, New York, 1982.